

Study on the Influence of the Splitter Blade Length on Radial and Axial Force of a Centrifugal Pump

Qijiang Ma^{1,2,3,4} ✉ – Zhenbo Liu⁴ – Sen Jiang⁵

¹ School of Mechanical and Electrical Engineering, Chuzhou University, China

² School of Mechanical Engineering, Hefei University of Technology, China

³ Anhui Liuxiang Special Ship Co., Ltd., China

⁴ National Research Center of Pumps, Jiangsu University, China

⁵ Ningbo Yi Ji Valve Manufacturing Co., Ltd., China

✉ qijma@chzu.edu.cn

Abstract To enhance the operational stability of centrifugal pumps, this study investigates the influence of splitter blade length on the axial and radial forces of centrifugal pumps. Using the SST $k-\omega$ turbulence model and experimental research, the external characteristics, axial force, radial force, and time-frequency characteristics of pressure pulsation were compared among impellers without splitter blades and those with splitter blades of two different lengths. The results show that impellers with a conventional structure achieve higher efficiency near the design operating point. However, under low-flow conditions, the rectifying effect of splitter blades allows impellers with splitter blades to achieve higher efficiency. For impellers with splitter blades, the axial force shows a periodic behavior, presenting two peak values – one large and one small – within each cycle. The addition of splitter blades shifts the radial force acting on the impeller to one side, requiring an increase in the support strength and stiffness of the rotor system. Furthermore, splitter blades influence the pressure pulsation at the impeller's inlet and outlet, the original impeller has an additional pulsation energy at 145 Hz but the splitter blades are different. Thus, an impeller with splitter blades can reduce the frequency pulsation and optimizing flow conditions. This study provides valuable theoretical insights and data support for the hydraulic structural optimization of centrifugal pumps.

Keywords centrifugal pump, axial force, radial force, splitter blade length, pressure fluctuation

Highlights

- Influence of splitter blade length on the axial and radial forces of centrifugal pump is studied.
- Impellers with a conventional structure achieve higher efficiency near the design operating point.
- Splitter blades shifts the radial force acting on the impeller to one side.
- Splitter blades influence the pressure pulsation at the impeller's inlet and outlet.

1 INTRODUCTION

Centrifugal pumps, as one of the most commonly used fluid transportation devices, are widely applied in various fields such as water treatment [1], chemical production [2], energy conversion [3], and agricultural irrigation [4]. Their operational efficiency and stability directly impact the economic viability and safety of production processes. The fundamental working principle of centrifugal pumps is based on the action of centrifugal force. By rotating, the impeller draws fluid from the pump inlet into the blades and accelerates it to a high specific velocity under centrifugal force, simultaneously converting kinetic energy into pressure energy [5]. As such, the impeller serves as the core component of a centrifugal pump.

In the design and operation of centrifugal pumps, dynamic characteristics are a critical factor that cannot be overlooked. Al-Obaidi used numerical calculation and experiment to study the complex hydrodynamic characteristics of axial flow pumps [6], including the influence of flow conditions [7], the influence of the number of blades [8], guide vane configurations [9], and the influence of cavitation characteristics [10]. Moreover, during operation, the blades are subjected to fluid dynamics forces, resulting in radial and axial forces [11]. Radial force primarily acts perpendicular to the rotational axis on the impeller and is caused by the centrifugal force of the fluid and the interaction between the impeller and the fluid. Axial force, on the other hand, is generated along the pump shaft

and is mainly influenced by the flow direction of the fluid within the pump. Notably, the inlet and outlet angles of the pump play a crucial role in the distribution of these forces [12]. Radial and axial forces are the primary factors affecting the stability of centrifugal pumps. Excessive radial force can increase friction between the pump casing and the impeller, leading to heat generation and localized wear [13]. Similarly, excessive axial force may cause bending of the pump shaft, compromising operational stability and reducing the pump's lifespan. Therefore, effectively controlling these forces is a key task in centrifugal pump design.

In recent years, advancements in computational fluid dynamics (CFD) have allowed researchers to delve deeper into the factors influencing radial and axial forces [14]. For instance, Zhu et al. [15] investigated the axial force of a guide vane mixed-flow pump using experimental and numerical simulation methods. They optimized the axial force by incorporating balance holes and balance disc structures, employing orthogonal experiments and BP neural network algorithms to achieve optimal efficiency and axial force. Liu et al. [16] studied the axial force characteristics of a centrifugal pump with a floating impeller structure, developing mathematical expressions for fluid leakage, fluid pressure, and axial force acting on a stainless steel disc in the axial gap. Their findings revealed that the floating impeller significantly reduces axial force. Dong et al. [17] examined the impact of particle flow on the axial force of a centrifugal pump, using a semi-open impeller pump as the study object. Their research showed that the total axial force in clear water conditions is greater

than in particle flow, but the total axial force increases as the solid-phase volume fraction rises. Cao et al. [18] investigated the influence of the backflow hole structure on the pump's axial force and energy characteristics, finding that when the ratio of backflow balance hole area to sealing ring area exceeds six, better axial force balance can be achieved. Similarly, significant progress has been made in the study of impeller radial forces. Cui et al. [19] explored the effect of radial force on the vibration characteristics of centrifugal pumps using numerical simulations to examine the relationship between flow rate, radial force, and vibration characteristics. Their results showed that impeller radial displacement aligns with radial force variations but lags behind in phase. Moreover, radial force-induced vibrations increase flow losses within the pump, reducing efficiency. González et al. [20] studied the impact of the clearance between the impeller and volute on radial forces in centrifugal pumps through experimental and numerical analysis of both steady and unsteady radial forces. They found that, under certain flow conditions, larger diameters generate higher radial forces, although this does not apply universally to all operating points. Ou et al. [21] conducted numerical studies on the hydrodynamic radial force in mixed-flow pumps, discovering that the transient hydrodynamic radial force of the impeller shows periodic variation over time. Under uniform inflow conditions, the average transient radial force approaches zero, while in certain flow conditions, recirculation flow structures significantly affect pressure pulsation and hydrodynamic radial force. The aforementioned studies highlight that the hydraulic structure of the impeller has a substantial impact on the axial and radial forces within the entire rotor system, further influencing the vibration and noise characteristics of the pump's operational system. Consequently, reducing axial and radial force pulsations has remained a key focus for both academia and industry.

In recent years, with advancements in the hydraulic design methods of centrifugal pumps, the splitter blade design approach has been introduced to enhance pump performance [22]. Splitter blades are secondary blades added behind the main flow path of the pump. By altering the flow path on the blades, they optimize the fluid flow state, reduce flow losses, and thus improve the performance and stability of the pump [23]. In centrifugal pumps, the design parameters for splitter blades are particularly critical. Different configurations of blade shape, length, and angle can lead to variations in fluid flow characteristics within the pump, thereby affecting the operational state and lifespan of the entire system [24]. For instance, Yan et al. [25] employed unsteady CFD analysis to enhance the efficiency of a double-volute centrifugal pump and reduce the unsteady radial forces on the impeller. By introducing splitter blades, they improved the pump's hydraulic performance and mitigated unstable radial forces. Similarly, Zeng et al. [26], aiming to reduce pressure and radial force pulsations at the design point of a centrifugal pump, considered the circumferential position, leading-edge location, and deflection angle of splitter blades. They demonstrated experimentally that splitter blades are effective in suppressing secondary flows and reducing fluid-induced vibrations. Xie et al. [27] studied the resonant response of impellers to multi-frequency fluid excitations using an acoustic-fluid-structure coupling method. They investigated the influence of the number and circumferential position of splitter blades on the natural frequency of impellers. Their findings revealed that adding splitter blades between the main impeller blades reduced the natural frequency of the impeller in both air and water, while the circumferential position of the splitter blades had minimal impact on the natural frequency. These studies collectively indicate that splitter blades significantly enhance the internal flow structure of pumps. However, the presence of splitter blades also influences the distribution characteristics of radial and axial forces on the impeller,

particularly with respect to blade length [28]. Existing research suggests that different blade lengths can alter the magnitude and distribution of radial and axial forces [29]. Appropriately designed blade lengths can not only improve pump efficiency and flow rate but also effectively reduce vortex flows within the pump, minimize noise, and enhance stability [30]. Conversely, improperly designed blade lengths may increase these forces, leading to greater vibrations, increased noise, and premature equipment wear [31]. While these findings primarily focus on the main blades of the impeller, they also provide valuable insights for the design of splitter blades. Currently, research on splitter blades remains limited, and studies specifically addressing the effects of splitter blade length on impeller axial and radial forces have yet to be published. Therefore, an in-depth investigation of the hydrodynamic characteristics of splitter blades and their impact on centrifugal pump performance not only offers guidance for pump optimization and improved energy efficiency but also provides critical theoretical and practical references for the development of related industries.

This study will employ a combination of experimental and numerical simulation methods. By constructing centrifugal pump models with varying blade lengths, the research will investigate the variations in radial and axial forces under different operating conditions. Numerical simulations will be conducted using CFD software to capture the actual fluid flow characteristics within the pump, and these results will be compared with experimental data. Simultaneously, the experimental data will be used to validate the accuracy of the simulation model and further analyze the impact of different design parameters on pump performance. This systematic research approach not only allows for a comprehensive analysis of the effects of blade length on the pump's dynamic characteristics but also provides practical guidance for future studies and applications.

2 METHODS & MATERIALS

2.1 Pump Model and Splitter Blade Structure

In this paper, we focus on the ISG25-220 model, a single-stage single-suction horizontal centrifugal pump, as our primary subject of research, illustrated in Fig. 1. The centrifugal pump is designed to have a flow rate (Q) of 88 m³/h, a head (H) of 12 m, and an operational speed (n) of 1450 rpm. For the design of the pump's hydraulic structure, we utilize a high-efficiency centrifugal pump model with a comparable specific speed, which is calculated as follows:

$$n_s = \frac{3.65n\sqrt{Q}}{H^{3/4}} = 21. \quad (1)$$

We primarily design two schemes: one with shunt blades and the other without, for comparative purposes. Additionally, to evaluate the impact of diverter blade length on the hydraulic performance of the centrifugal pump, we implement two different lengths of diverter blades for further analysis. Consequently, three distinct hydraulic design schemes for the impeller are selected, as depicted in Fig. 2.



Fig. 1. Physical centrifugal pump model

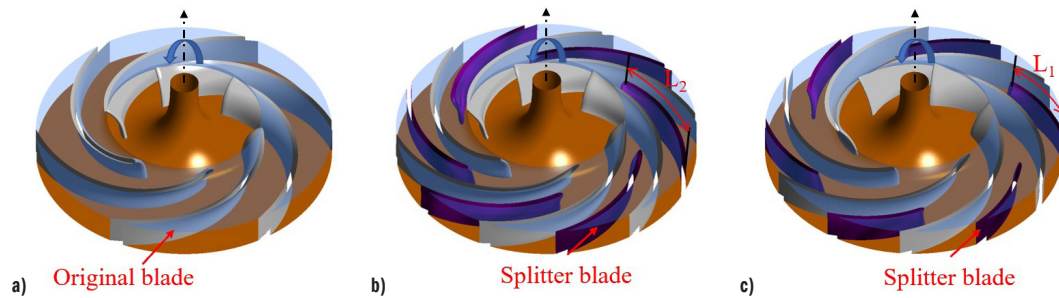


Fig. 2. Splitter blades structure; a) impeller #A, b) impeller #B, c) impeller #C

The rotary bias method is mainly used in the design of the shunt blade. Since the original non-shunt impeller has 6 blades, the angle between each blade is 60° . Therefore, when designing the splitter blade, the original blade is rotated by 30° and its inlet edge is cut, leaving only the tail of the blade. In this paper, the length of the splitter blade is set to 0.7 times and 0.3 times of the original blade length respectively. The main parameters of the centrifugal pump model and the splitter blade are shown in Table 1.

Table 1. Main parameters of the centrifugal pump model

Parameter	Value
Designed flow rate, Q_d [m ³ /h]	88
Designed rated head, H [m]	12
Rated speed, n [rev/min]	1450
Impeller inlet diameter, D_1 [mm]	112.5
Impeller outer diameter, D_2 [mm]	219
Number of blades, Z	6
Impeller outlet width, b_2 [mm]	22.02
Blade inlet angle, β_1 [°]	
Blade outlet angle, β_2 [°]	16.5
Blade wrap angle, ϕ [°]	90
Guide vane angle, α [°]	15
Volute base circle diameter, D_3 [mm]	176.5
Volute outlet diameter, D_4 [mm]	100

2.2 Pre-Processing of Numerical Calculation

Some preparatory work is required before numerical calculations are performed on a centrifugal pump model. The first is to model the computational domain through 3D design software. The hydraulic power of the model pump was modeled by UG NX software in three dimensions, including inlet section, outlet section, impeller, volute and pump gap chamber. In the three schemes in this paper, the clearance of the impeller mouth ring is equal and has little influence on the flow field in the shunt impeller, so it can be ignored in the modeling process. In addition, considering that inlet reflux and outlet reflux will lead to divergence of the calculation process, the inlet and outlet areas of the impeller are extended respectively [32]. The three-dimensional water structure of the centrifugal pump is shown in Fig. 3.

Grid is the carrier of simulation and analysis, and the quality of grid has an important impact on the calculation accuracy and efficiency [33]. In this paper, ANSYS ICEM is used to divide the hexahedral structure of the whole basin. In the process of discretization of the calculation domain, the mixed mesh method is mainly adopted, that is, hexahedral structured mesh is mainly used for the inlet segment, outlet segment, volute and pump cavity, which can not only accurately control the streamline distribution and the orthogonal direction of the boundary layer, but also flexibly adjust

the distance between nodes to adjust the density of the boundary layer mesh [34]. As for the impeller, due to its high hydraulic structure complexity, the generated hexahedral mesh quality is poor, so the tetrahedral unstructured mesh is used to generate. For the three impeller schemes that need to be compared in this paper, the same mesh generation standard is adopted, and the final mesh quality is higher than 0.5. Figure 3 shows the meshing scheme and encryption details for different computing domains.

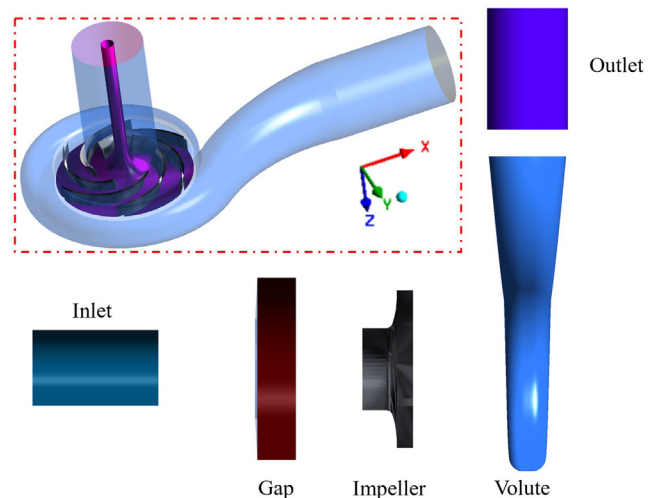


Fig. 3. Mesh generation detail of the pump model

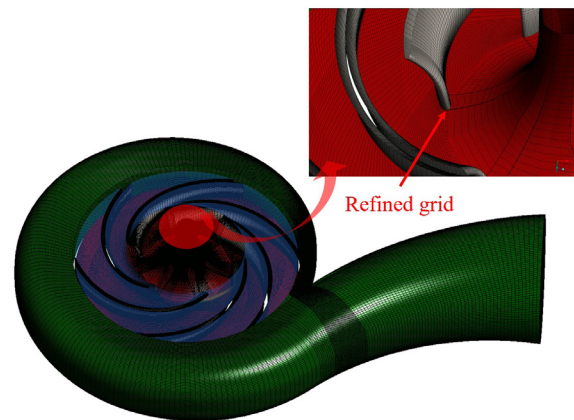


Fig. 4. Mesh details of different simulation domain

The presence of boundary layer mesh can more accurately capture the flow in the near-wall region and reflect the flow characteristics in the near-wall region [35]. Thus, it is necessary to encrypt the boundary layer of blade surface and volute tongue to ensure calculation accuracy. In order to meet the requirements of different flow patterns on the number of grids in the near wall area, in order

to ensure that there are enough nodes in the area, y^+ value can be used to test the location of the node closest to the wall. Here, y^+ value represents the distance from the node closest to the wall to the wall, and is a dimensionless variable, whose definition is as follows [36]:

$$y^+ = \frac{uy}{\nu}, \quad (2)$$

where, u represents the wall friction velocity, [m/s]; y represents the distance between the two nodes closest to the wall, [m]; ν represents kinematic viscosity, [Pa·s]. The y^+ values of blade surface and volute wall are shown in Fig. 5.

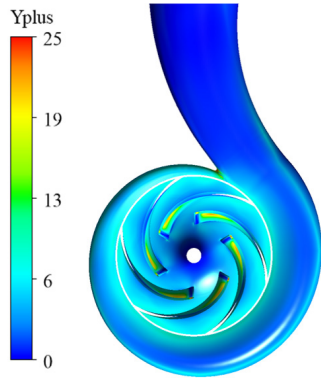


Fig. 5. Distribution of y^+ on the blade

2.2 Grid Independence Test

In the numerical calculation, it is necessary to analyze the influence of the number of grids on the calculation results to avoid the solution error caused by the size of the grid, that is, the number of grids [37]. Thus, it is necessary to use different mesh sizes for grid division. The grid independence analysis is carried out based on the change of the head with the number of grids under the design condition, and an appropriate number of grids is selected for further study.

To evaluate the sensitivity of the computational mesh, this study adopts the grid convergence index (GCI), a method initially introduced by Li et al. [38]. The GCI approach necessitates that the obtained results adhere to the condition of monotonic convergence to ensure reliability. In this work, three distinct grids with varying levels of refinement were constructed and analyzed under the rated operating conditions of the original impeller design. This process enables a systematic assessment of how mesh resolution influences the accuracy and stability of the simulation results. The formula for calculating GCI is as follow [39]:

$$GCI = \frac{|F_s| \alpha_{b+1,b}}{r_{b+1,b}^p - 1}, \quad (3)$$

where F_s is the safety factor, taking values in the range 1.25 to 3.00, and 1.25 when three or more grids are used.

Symbol r denotes the grid refinement ratio and is defined as follows:

$$r_{b+1,b} = \left(\frac{N_{b+1}}{N_b} \right)^{\frac{1}{D}}, \quad (4)$$

where N is the number of control cells of the grid; D is the computational dimension; the subscript b represents different grid schemes, with larger b indicating a denser grid.

Symbol φ is the relative error of the results obtained from numerical calculations using two sets of grids with adjacent quantities:

$$\alpha_{b+1,b} = \left| \frac{f_b - f_{b+1}}{f_{b+1}} \right|, \quad (5)$$

where f_b is the numerical discrete solution of the selected convergence parameter.

Symbol κ is the convergence accuracy. When three sets of grids are used for GCI analysis, κ can be calculated iteratively based on Eq. (6) as follows:

$$\beta = \frac{1}{\ln(r_{2,1})} \left| \ln \left(\frac{f_3 - f_2}{f_2 - f_1} \right) + g(\beta) \right|, \quad (6a)$$

$$g(\beta) = \ln \left(\frac{r_{2,1}^\beta - s}{r_{3,2}^\beta - s} \right), \quad (6b)$$

$$s = \text{sgn} \left(\frac{f_3 - f_2}{f_2 - f_1} \right), \quad (6c)$$

where $g(\kappa)$ is the κ -order error term coefficient that does not vary with the grid. It should be noted that when $(f_3 - f_2)/(f_2 - f_1) < 0$, i.e., $s = -1$, the oscillatory iterative convergence solution is prone to occur, and then the grid needs to be replaced and recreated.

As can be seen from Table 2, with the increase of the number of grids, the value of GCI decreases from 1.21 % to 0.62 %, meeting the requirement that the value required by the GCI convergence standard is less than 1. Therefore, in the final calculation scheme, the grid density scheme is selected for grid generation in all calculation domains.

Table 2. Calculated results of GCI with different sizes of grids

Mesh number $\times 10^6$	Relative error	GCI [%]
20.3	0.000097	1.21
23.6		
30.5	0.000034	0.62

2.2 Governing Equations and Boundary Conditions

The numerical calculation process of the flow field in centrifugal pump is actually a process of solving the governing equation, and in order to solve the governing equation, it is necessary to select a suitable turbulence model closed equations. Reynolds time average method uses time mean value and pulsation value to represent instantaneous value, which has high reliability and small calculation amount, and can basically meet the engineering application requirements, so it is the most widely used in practical engineering [40]. The turbulence model based on Reynolds-averaged Navier–Stokes (RANS) equation can be divided into vortex viscosity model and Reynolds stress model. The vortex viscosity model is mainly used to solve the turbulence viscosity coefficient, which can be divided into zero equation model, single equation model and two-sided equation model, among which the two-sided equation model is the most widely used. The standard Reynolds stress model is mainly used to solve the Reynolds stress transport equation [41]. Because the SST $k-\omega$ model uses a mixed function combining the standard $k-\omega$ and the transformed $k-\varepsilon$ model, the standard $k-\omega$ model is used in the near wall region and the transformed $k-\varepsilon$ model is used away from the near wall region. At the same time, considering the transmission of turbulent shear force in the internal flow field, the flow separation amount of fluid under negative pressure gradient can be predicted very accurately, without excessive prediction of eddy viscosity, which is especially suitable for the simulation of boundary layer requiring high precision. Therefore, the SST $k-\omega$ model closed control equations are used in this paper to numerically calculate the internal flow field of low specific speed centrifugal pump under different working conditions.

In the SST k - ω model, the eddy viscosity coefficient and k equation and k equation are expressed as

$$\frac{\partial(\rho k)}{\partial t} + \frac{\partial(\rho k u_i)}{\partial x_i} = \frac{\partial}{\partial x_j} \left[\left(\mu + \frac{\mu_t}{\sigma_{k3}} \right) \frac{\partial k}{\partial x_j} \right] + P_k - \beta^* \rho k \omega, \quad (7)$$

$$\frac{\partial(\rho \omega)}{\partial t} + \frac{\partial(\rho \omega u_i)}{\partial x_i} = \frac{\partial}{\partial x_j} \left[\left(\mu + \frac{\mu_t}{\sigma_{\omega 3}} \right) \frac{\partial \omega}{\partial x_j} \right] + \alpha_3 \frac{\omega}{k} P_k - \beta_3 \rho \omega^2 + 2(1 - F_1) \rho \frac{1}{\omega \sigma_{\omega 2}} \frac{\partial k}{\partial x_j} \frac{\partial \omega}{\partial x_j}, \quad (8)$$

$$\mu_t = \rho \frac{a_1 k}{\max(a_1 \omega, S F_2)}, \quad (9)$$

$$P_k = \mu_t \left(\frac{\partial u_i}{\partial x_j} + \frac{\partial u_j}{\partial x_i} \right) \frac{\partial u_i}{\partial x_j} - \frac{2}{3} \frac{\partial u_k}{\partial x_k} \left(3 \mu_t \frac{\partial u_k}{\partial x_k} + \rho k \right), \quad (10)$$

where, F_1 and F_2 serve as blending functions within the SST k - ω turbulence model, while S denotes the shear force constant. The model utilizes an empirical constant β , specifically set to 0.09, alongside a_1 , another empirical constant. The turbulent eddy frequency, ω [s^{-1}], while the turbulent kinetic energy, k [m^2/s^2]. These parameters work together to accurately represent and predict flow behavior within the model's two-equation framework.

The setting of boundary conditions will essentially affect the accuracy of the calculation results. The steady conditions of the low specific speed centrifugal pump model are set as follows: the inlet boundary condition is set as the total pressure, the outlet boundary condition is set as the mass flow, the impeller is set as the frozen rotor when it contacts with the inlet section and the impeller and the volute, and the rotation Angle is specified as 360° . Set the number of steady calculation steps of the model to 2500. The unsteady setting of the outlet and inlet of the model is the same as that of the steady setting. The difference is that the impeller wall is set to instantaneous rotation, the inlet of the impeller and the contact surface between the volute and the impeller are set to instantaneous freezing rotor total time 0.103448 s, and the time step is $t = 1.72414 \times 10^{-4}$ s, that is, the impeller of the centrifugal pump model rotates 5 times. The impeller is turned 3° at each time step. To ensure simulation accuracy, a convergence criterion of 10^{-4} was selected for both the continuity and momentum equations.

2.3 Experimental Equipment

Based on the open test bench of Zhenjiang Machinery, China industry testing institution, the performance test of the pump was carried out. Figure 4 shows a schematic diagram of the test bench. First let the motor no load, torque calibration at rated speed, and then connect the motor to the test pump shaft. Connect each test device and instrument according to the test standard, then fill the test pipe with normal temperature water, turn on the machine to check whether the instrument and equipment can work normally, open the pipe vent, and drain the air in the pipe. Before starting the test mixed-flow pump, the inlet and outlet valves on the test pipe are adjusted to the maximum opening, and then the speed is adjusted by the frequency conversion regulator to make the speed reach and maintain at the rated speed of 1450 r/min.

Keep the inlet valve open to the maximum, slowly reduce the outlet valve open, parameter measurement under different flow conditions. Observe the indicator number on the pump product parameter measuring instrument and system analysis program. When the indicator number is stable at a certain value or fluctuates back and forth within a small range of a certain value, it is considered as the measured value and the corresponding data is recorded. After the data measurement of the minimum flow condition is completed, the speed is still adjusted by the variable frequency regulator to slowly reduce to zero. After the shutdown is complete, wait for the water flow in the pipeline to stop, and then turn the outlet valve open to the maximum again. In order to minimize the accidental error and improve the reliability of the test data, the energy characteristic data recorded in the three repeated tests were arithmetically averaged and used as the final test result.

2.4 Verification of Simulation

The pump data acquisition terminal and processing program can calculate the head of the test pump according to the inlet and outlet pressure of the test pipeline, the shaft power can be calculated according to the torque and speed data measured by the torque and speed measuring instrument, and the efficiency can be calculated according to the head and shaft power. The three expressions are as follows:

$$H = Z_2 - Z_1 + \left(\frac{p_2 - p_1}{\rho g} \right) + \left(\frac{v_2^2 - v_1^2}{2g} \right), \quad (11)$$

$$P = \frac{n \cdot (M - M_0)}{9552}, \quad (12)$$

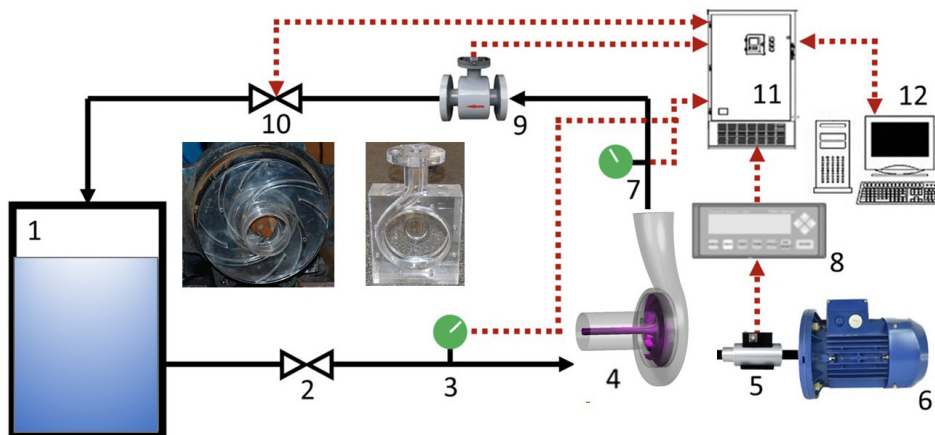


Fig. 6. Schematic diagram of experiment system; 1 water tank, 2 valve, 3 inlet pressure transmitter, 4 pump, 5 torque sensor, 6 motor, 7 outlet pressure transmitter, 8 torque speed transmitter, 9 flowmeter, 10 valve, 11 data acquisition terminal, and 12 computer

$$\eta = \frac{\rho g Q H}{1000 P} \times 100 \% \quad (13)$$

In Equation (11), p_1 and p_2 are respectively pump inlet and outlet pressure, [Pa]; Z_1 and Z_2 are the installation heights of pump inlet and outlet respectively, [m]. In this test, the installation heights of pump inlet and outlet are the same, so $Z_1 = Z_2$; v_1 and v_2 are respectively the average flow rate of the inlet and outlet of the pump, [m/s], which can be calculated from the inner diameter of the inlet and outlet pipeline; M is the measured torque of the pump set, M_0 is the no-load torque, [N·m]; n is the speed, [r/min]; Q is the flow rate, [m³/h]; H is the head, [m]; P is the shaft power of the mixed flow pump, [kW].

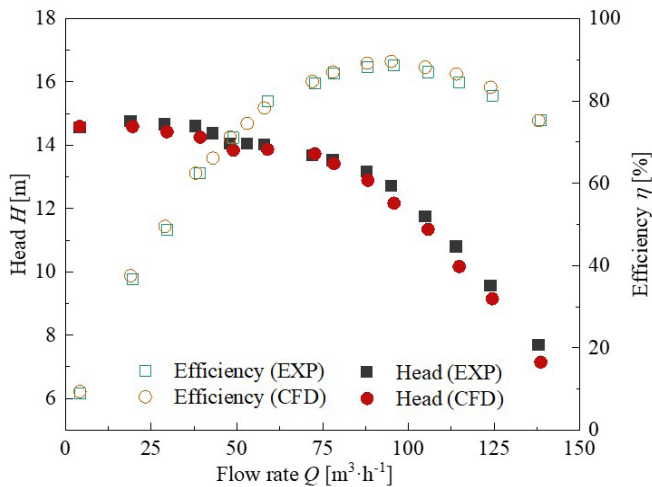


Fig. 7. Comparison of simulations and experimental results

Figure 6 shows the performance curves obtained from numerical calculations and tests of the model pump. From the trend of the head and efficiency, the numerical and experimental results are in perfect agreement. At about $Q=95$ m³/h, the efficiency of the centrifugal pump has the maximum value and is the optimal working condition point. With the decrease in flow condition, the head curve gradually increases. At about $Q=45$ m³/h, the local lowest point of the lift curve appears, which is the point of stall condition, but the drop of the lift is not much, indicating that the flow loss is not serious. From the overall change of the head and efficiency, the head curve changes gently in the low flow condition, indicating that the flow

structure in the pump shows a certain trend change. By comparing the experimental and numerical results, it can be found that the error between the numerical results and the experimental values is less than 10 % under each flow condition, and further the error is under 0.2 for each test, which meets the accuracy required by the numerical calculation. Therefore, the numerical method adopted in this paper is feasible.

3 RESULTS AND DISCUSSION

3.1 Comparison of Energy Performance

Figure 8 compares the head and efficiency curves of centrifugal pumps with and without splitter blades. The results reveal that pumps with splitter blades exhibit distinct performance characteristics compared to conventional impellers, especially under low-flow operating conditions. Unlike the consistent negative slope observed in conventional impellers, the head curve of pumps with splitter blades transitions from a negative slope to a positive slope, indicating the presence of a noticeable extremum point. In terms of specific head values, centrifugal pumps equipped with splitter blades achieve significantly higher head performance than conventional impellers. It is almost 8 % higher than the original impeller design under the condition of 70 m³/h. For longer splitter blade structures, the head is slightly higher, although the difference is marginal. Regarding efficiency curves, conventional impellers demonstrate higher efficiency near the design operating point, whereas impellers with splitter blades achieve better efficiency under low-flow conditions due to the rectifying effect of the splitter blades. Consequently, while splitter blades positively influence the head curve of centrifugal pumps, this enhancement comes at the cost of some efficiency loss.

3.2 Analysis of Flow Field of Centrifugal Pump Blades with Different Splitter Blade Length

Figures 9 and 10 illustrate the pressure and velocity distributions within the impeller for different impeller designs. As shown in the figures, both pressure and velocity are relatively low at the impeller inlet but gradually increase as the fluid moves toward the impeller outlet, reaching their peak values at the exit. Comparing different impeller designs, it is evident that the addition of splitter blades results in a more uniform pressure distribution along the impeller

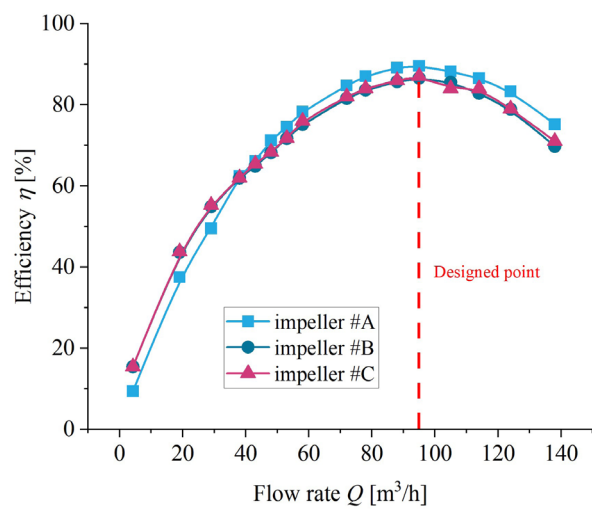
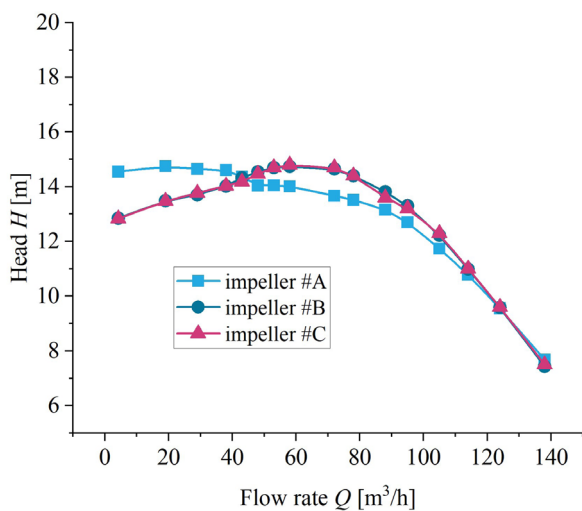


Fig. 8. Impact on the pump performance of splitter blades; a) head, and b) efficiency



Fig. 9. Pressure distribution in different kinds of impeller

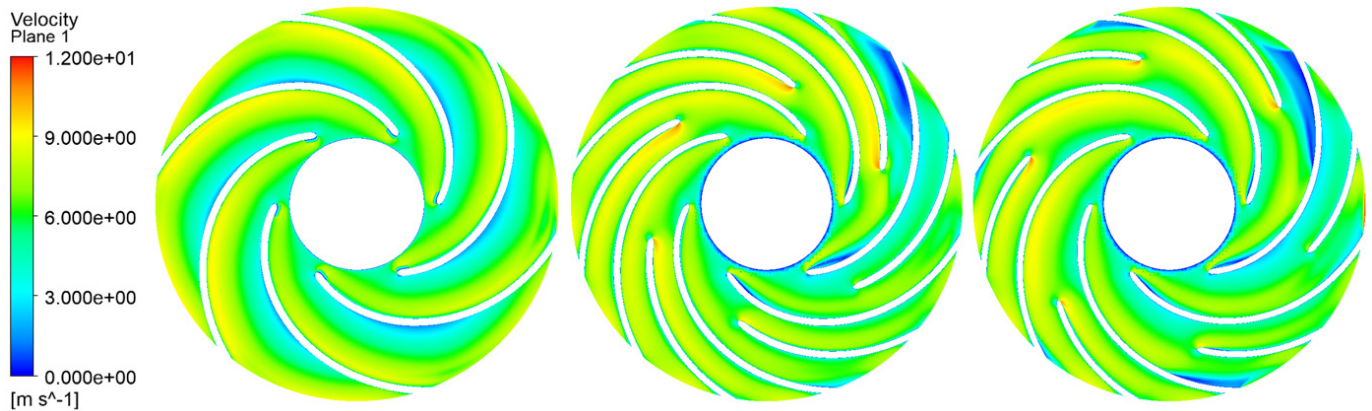


Fig. 10. Velocity distribution in different kinds of impeller

periphery. Notably, near the volute tongue, the high-pressure region is significantly reduced, and the circumferential pressure uniformity is improved. This explains why the splitter blades contribute to a higher head in the centrifugal pump. However, the introduction of splitter blades also leads to the formation of a distinct low-velocity region near the tongue, which plays a crucial role in the development of vortex structures. The presence of these vortices increases hydraulic losses within the pump, ultimately leading to a reduction in efficiency under the design operating conditions.

3.3 Analysis of Axial Force of Centrifugal Pump Blades with Different Splitter Blade Length

Figure 10 illustrates the schematic diagram of the axial force acting on the impeller of the centrifugal pump under design operating condition. According to the pump fluid dynamics theory, the axial force of the impeller primarily originates from the fluid within the impeller flow passage and the fluid in the gaps between the front and rear shrouds of the impeller. Zhu et al. [42], developed a mathematical model of the axial force exerted on the impeller by the fluid in the front and rear gap regions under the rotational action of the impeller. The main expression of the model is as follows:

$$F^* = -F_1^* + F_2^* = -\int_{r_1}^{r_0} 2\pi r \cdot P \cdot \frac{1}{2} \rho r_0^2 \omega^2 dr + \int_{r_2}^{r_0} 2\pi r \cdot P \cdot \frac{1}{2} \rho r_0^2 \omega^2 dr. \quad (14)$$

Here, F_1 represents the axial force acting on the front shroud of the impeller, while F_2 denotes the axial force acting on the rear shroud. However, this model only accounts for the axial force caused

by the gap fluid and needs to include the contribution of the fluid within the impeller flow passage to represent the total axial force acting on the impeller. Although some researchers have proposed empirical formulas to calculate the axial force caused by the fluid within the impeller flow passage, in this study, more accurate axial force values can be directly obtained through post-processing in simulation software. Therefore, the final axial force is the sum of three components: the axial force on the front shroud, the axial force on the rear shroud, and the axial force caused by the fluid within the impeller flow passage.

Figure 12 presents the time-dependent variations in the axial force acting on the impeller under design conditions for different impeller structures. To minimize random errors, the axial force over the last three revolutions at the same impeller phase was averaged arithmetically. Additionally, the axial forces for different flow field phases of the two splitter blade configurations were compared, with specific time points marked in the Fig. 12. Since the splitter blades are only located within the impeller flow passage, they do not affect the fluid in the gaps between the front and rear shrouds. Consequently, the axial force exerted by the splitter blades has only the flow passage component. From Fig. 10, it is observed that for the original impeller, the axial force shows a periodic variation over time, with a time interval of approximately 0.0069 s between two peak values, equivalent to 20-time steps. Moreover, the axial force is negative, indicating that its direction is toward the impeller inlet. The maximum axial force is approximately 114 N, while the minimum is around 62 N, nearly doubling within a single cycle. This suggests that the impeller is susceptible to fluid excitation forces during pump operation, potentially leading to vibrations. In contrast, for the impellers with splitter blades, the magnitude of the

axial force is significantly increased, but periodic behaviors similar to the original impeller are observed, with the same periodic interval. However, in this case, two peaks – one large and one small – are present within a single cycle, which is distinct from the original impeller. Additionally, the axial force direction for both splitter blade configurations remains the same as that of the original impeller. As the length of the splitter blades decreases, the axial force slightly increases, rising from approximately 149 N to 170 N. However, in terms of relative fluctuation amplitude, the increase in axial force is significantly reduced. This indicates that splitter blades play a role in mitigating axial vibrations of the impeller.

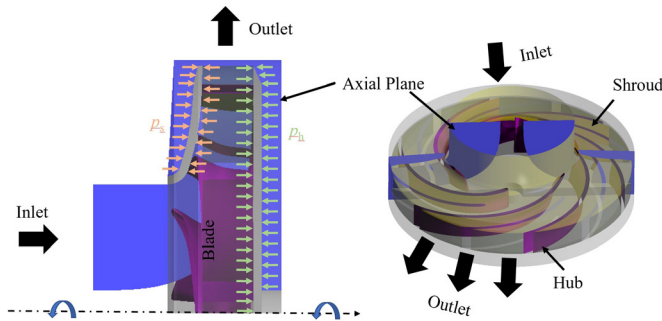


Fig. 11. Axial force diagram of impeller

3.4 Analysis of Radial Force of Centrifugal Pump Impeller with Different Splitter Blade Lengths

Figure 13 shows the curves of the radial force acting on the impeller varying with time under different design conditions. Meanwhile, the radial force fluctuation curve within one impeller rotation period was selected and its schematic distribution along the circumference of the impeller was plotted, as shown in Fig. 14. It can be seen from the figures that the impellers under the three types of structures all exhibit certain radial force fluctuation characteristics, but the fluctuation characteristics of the original impeller and the impeller with splitter blades are significantly different. For the original impeller, the radial force pulsation curve has a more pronounced periodicity, with only one peak value within one period. However, for the impeller with splitter blades, the periodicity of the radial force is weakened. Comparing impeller #B and impeller #C, it can be seen that the difference in the extremes of the radial force over multiple rotation periods is large, exceeding 40 N, which is much greater than the radial force pulsation value under the design condition. This indicates that the existence of the splitter blades leads to a serious imbalance of the radial forces. From Figure 12, it can also be seen that the radial force on the original impeller shows a central symmetric structure along the rotation axis, but for impeller #B and impeller #C impellers, this pattern is broken, and the radial force acting on the impeller is biased to one side. This requires the rotor bearings of the centrifugal pump to have the ability to withstand larger support forces in order to reduce the radial excursion of the impeller during rotation and maintain relative stability. Therefore, in the actual pump design process, when splitter blades are added to the impeller, the support stiffness and strength of the rotor system bearings need to be further improved.

3.5 Analysis of Pressure Pulsation Characteristics in Impeller with Different Blade Structures

To further clarify the influence of different impeller structures on the pressure pulsation characteristics within the pump, this section obtained the time-domain and frequency-domain distribution curves

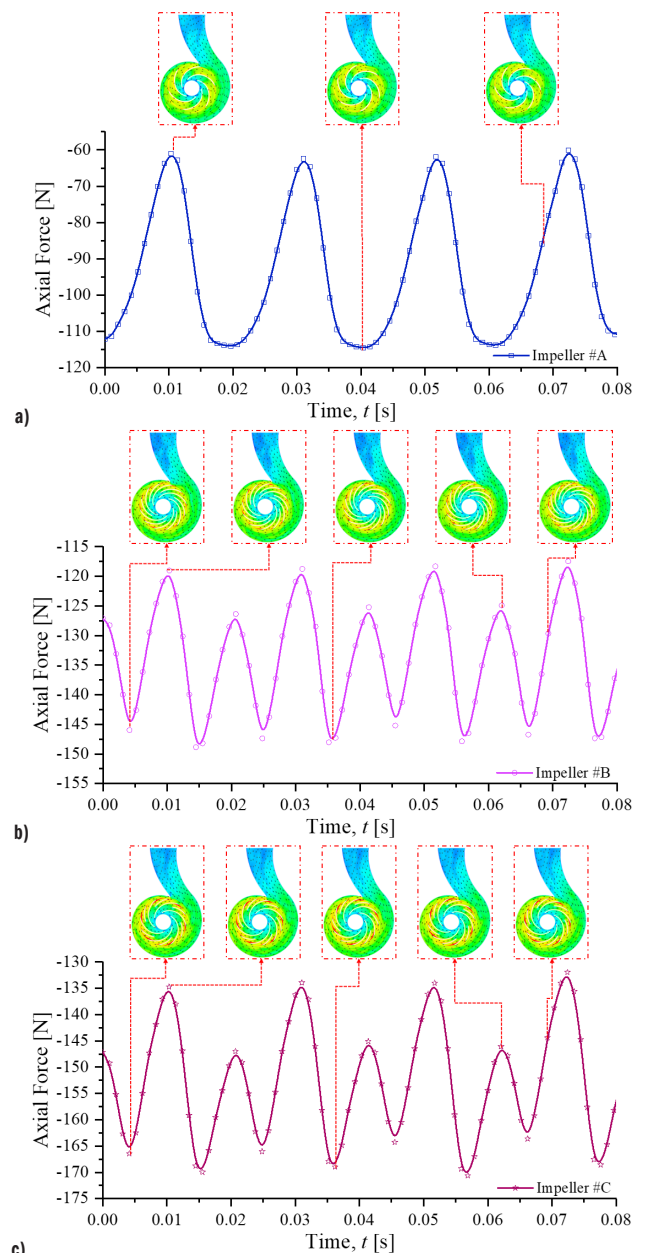


Fig. 12. Variation trend of axial force on impeller with time under different impeller structures; a) impeller #A, b) impeller #B, and c) impeller #C

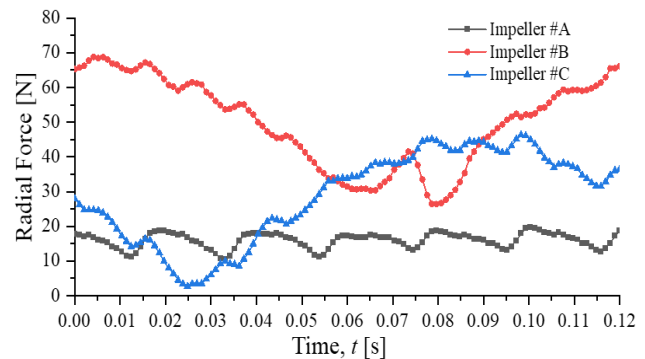


Fig. 13. Variation trend diagram of radial force on impeller with time under different impeller structures

of pressure pulsation at three locations in the centrifugal pump under the design condition for different impeller structures. The locations

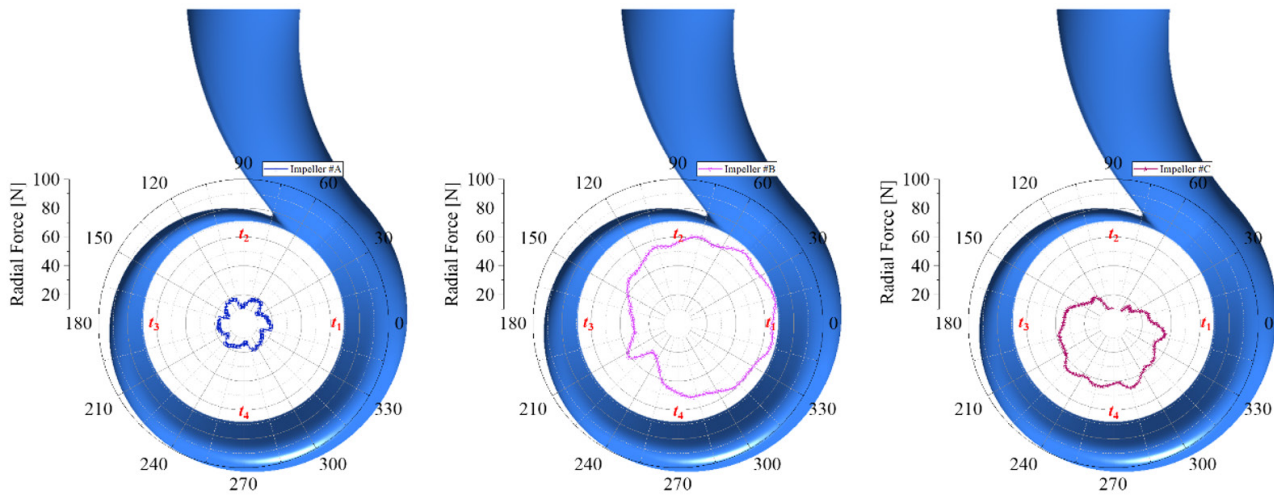


Fig. 14. Circumferential distribution of radial force of impeller

of the three pressure monitoring points are shown in Fig. 15. The time-domain diagrams of the pressure pulsation are shown in Fig. 16. To reduce the random error, this paper selected the dimensionless pressure coefficient C_p for comparison, which is defined as:

$$C_p = \frac{\left(\sum_{i=1}^N p \right) / N}{\frac{1}{2} \rho U^2}, \quad (15)$$

where p is the instantaneous pressure at the monitoring point, [Pa]; U is the peripheral velocity at the impeller outlet, [m/s].

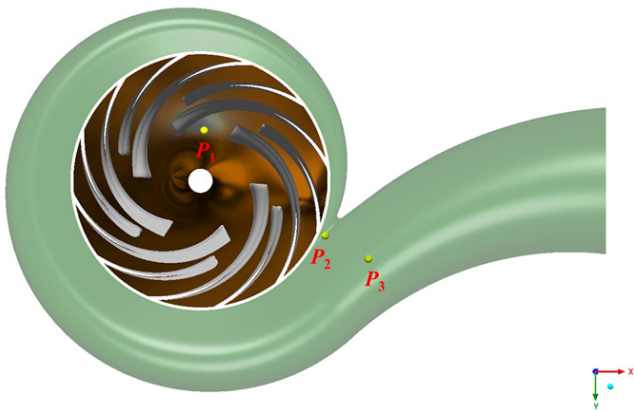


Fig. 15. Schematic diagram of the location of pressure monitoring points

From the analysis of Fig. 14, it can be seen that at the impeller inlet (P_1), the pressure pulsation curves for the three impeller structures all exhibit a certain periodicity, but within the same period, the original impeller has fewer oscillations than impeller #B and impeller #C, which is related to the number of blades. Although the splitter blades are added downstream of the impeller flow passage, they still have an influence on the pressure fluctuations at the impeller inlet. Additionally, the pulsation amplitude of the original impeller is significantly higher than that of impeller #B and impeller #C. The pulsation coefficient C_p of the original impeller reaches 0.3, while the pressure coefficients of the two diffuser blade impellers are both less than 0.2. This indicates that the flow at the impeller inlet becomes more stable after adding the splitter blades. At the impeller outlet (P_2), the periodicity of the pressure pulsation curves still exists for the three impeller structures, but the extreme value of the

pulsation coefficient for the original impeller is still slightly higher than the two diffuser blade impeller structures. This suggests that the flow stability at the outlet of impeller #B and impeller #C remains better. In the middle of the volute outlet pipe (P_3), the pressure pulsation characteristics for the three impeller structures do not show significant differences, as this location is far away from the impeller and less influenced by the impeller.

To further extract the characteristics of pressure pulsation, the time-domain signals at each monitoring point were subjected to fast Fourier transform (FFT) to obtain the frequency-domain distribution shown in Fig. 17. From the figure, it can be seen that at the impeller inlet, the dominant frequency of the original impeller is 145 Hz, which is the blade passing frequency of the original impeller. Furthermore, the pulsation amplitude at the dominant frequency of the original impeller is the highest, followed by the second harmonic, and the third harmonic is further reduced. This phenomenon indicates that the energy at the inlet and outlet of the original impeller gradually attenuates with increasing frequency. For the two impeller structures with splitter blades, their dominant frequency is 300 Hz, which is twice the blade passing frequency of the original impeller. This is due to the addition of the splitter blades. In other words, the blade passing frequency of the splitter blades is twice that of the original impeller blades. In this case, the energy at the dominant frequency of the splitter blades is predominant, while the energy at other harmonics is relatively small. Ignoring the other harmonic energies and only comparing the blade passing frequency and the energy at twice the frequency among the three impellers, it can be found that the amplitudes at 300 Hz are not significantly different, but the original impeller has an additional pulsation energy at 145 Hz. This further indicates that the impeller with splitter blades can reduce the frequency pulsation at the impeller inlet and promote more stable flow. Comparing impeller #B and impeller #C, it can be found that the amplitude at the dominant frequency is slightly lower for impeller #C, which also suggests that the length of the splitter blades is an important factor affecting the pulsation at the impeller inlet.

At the impeller outlet, the frequency amplitudes for the three impellers have all decreased. The main frequency characteristics of the impellers with splitter blades are the same as at the impeller inlet, with the blade passing frequency still dominating, but the energy at twice the blade passing frequency is significantly increased. This indicates that the flow structure at the impeller outlet becomes more unstable, which is consistent with the physical reality. At this point, the dominant frequency of the original impeller is still the

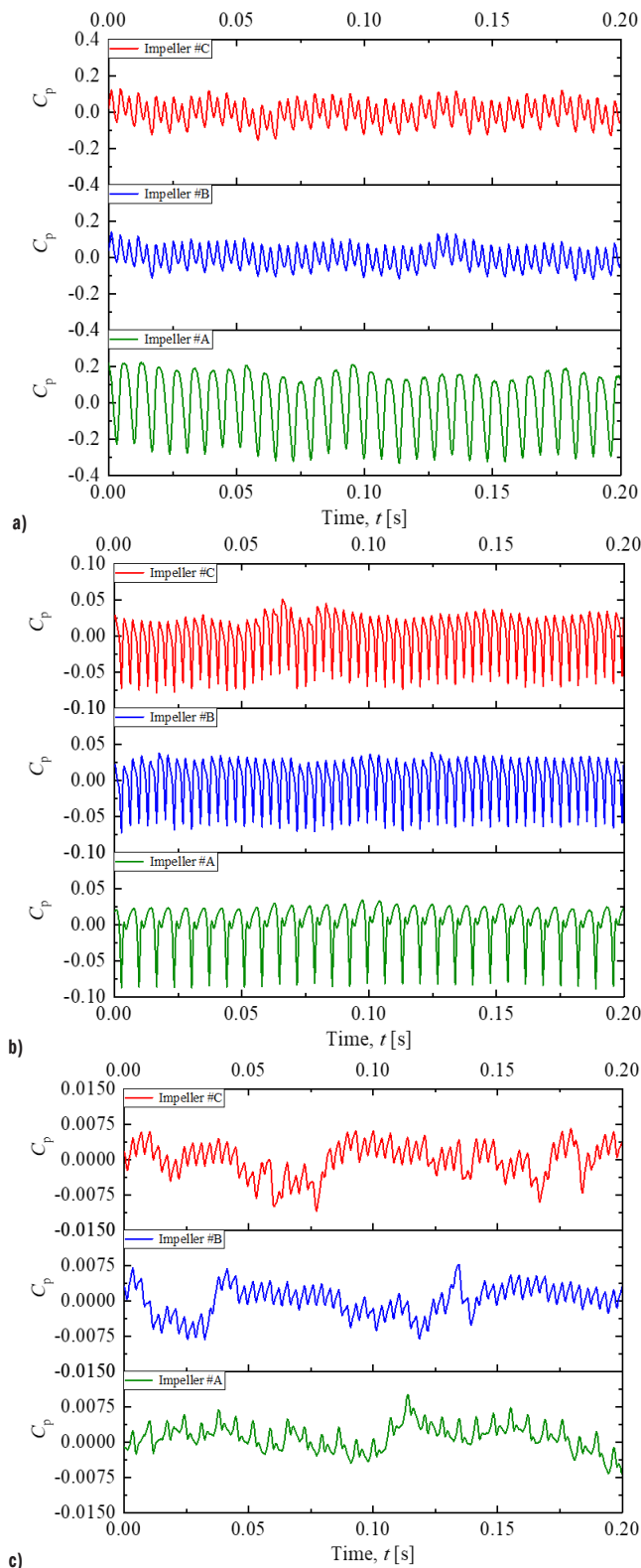


Fig. 16. Time domain of monitoring points at designed point; a) point P_1 , b) P_2 , and c) P_3

blade passing frequency, but the energy at the second, third, and fourth harmonics gradually decreases, which is different from the rapid attenuation of the harmonic energy at the impeller inlet. Under different diffuser blade lengths, the shorter splitter blades have lower dominant frequency energy, and the flow condition is slightly better than the longer splitter blades. At the volute outlet, the frequency

characteristics of the three impellers do not differ significantly, with the dominant frequency energy concentrated at low frequencies, which is due to the unsteady flow structure at the volute outlet. In this case, the length of the splitter blades does not have a noticeable impact on the flow field at this location. Therefore, from the pressure pulsation frequency response at different locations, it can be further understood that the splitter blades can reduce the amplitude of the dominant frequency at the impeller inlet, optimize the flow structure at the impeller inlet and outlet, but the influence of the splitter blades on the flow structure within the volute is not significant.

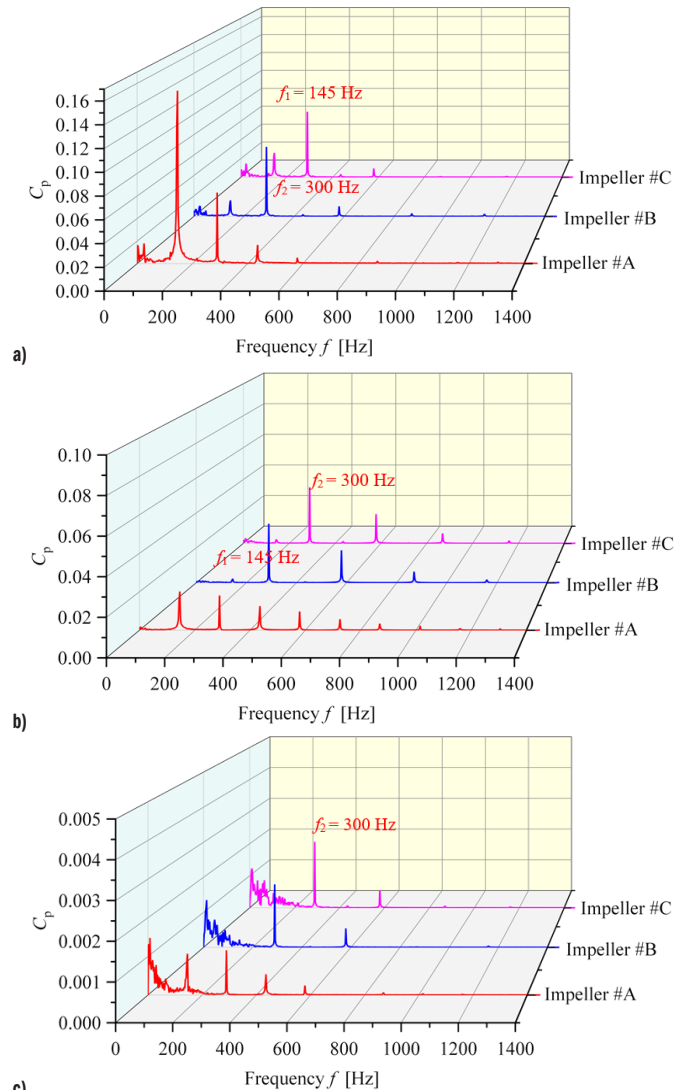


Fig. 17. Frequency domain of monitoring points at designed point; a) point P_1 , b) P_2 , and c) P_3

4 CONCLUSIONS

The performance of pumps with splitter blades is significantly different from ordinary impellers, especially in the low flow rate operating range. The head curve of a centrifugal pump with splitter blades has a distinct peak, and there is a positively sloped region at low flow rates. The head is almost 8 % higher under low flow rate while the efficiency of the ordinary impeller structure is higher near the design operating point, but at low flow rates, the straightening effect of the splitter blades gives the impeller with splitter blades a higher efficiency.

For the impeller structure with splitter blades, the axial force on the impeller shows a certain periodicity, with the same time interval as the impeller structure without splitter blades. However, within one period, the axial force on the impeller with splitter blades has two peak values – one large and one small. The length of the splitter blades can also affect the magnitude of the axial force, and can help reduce the axial vibration of the impeller.

After adding the splitter blades, the original radially symmetric force distribution on the impeller is changed, and the radial force acting on the impeller becomes biased to one side. This requires an increase in the support strength and stiffness of the rotor system. Additionally, the splitter blades can influence the pressure pulsation at the impeller inlet and outlet, optimizing the flow conditions, but their impact on the flow structure within the volute is not significant.

This article provides an in-depth analysis of the impact of splitter blade length on the axial and radial forces of a centrifugal pump. The findings are highly significant for optimizing pump design, enhancing operational stability, and extending service life under various working conditions. Future research should further explore the effects of the placement angle, degree of distortion, and number of splitter blades on pump performance to provide more comprehensive design guidance for centrifugal pumps.

References

- [1] Pu, W., Ji, L., Li, W., Shi, W., Tian, F., Xiao, C. et al. Study on the particle dynamic characteristics in a centrifugal pump based on an improved computational fluid dynamics-discrete element model. *Phys Fluids* 36 123331 (2024) DOI:10.1063/5.0242078.
- [2] Pu, W., Ji, L., Li, W., Yang, Q., Liu, Z., Yang, Y. et al. Experimental study on the unsteady evolution mechanism of centrifugal pump impeller wake under solid-liquid two-phase conditions: Impact of particle concentration. *Phys Fluids* 36 113327 (2024) DOI:10.1063/5.0239240.
- [3] Ji, L., Pu, W., Li, W., Shi, W., Yang, Y., Xiao, C. et al. PIV experimental study on dynamic and static interference flow field of multi-operating centrifugal pump under the influence of impeller wake. *Exp Therm Fluid Sci* 161 111355 (2024) DOI:10.1016/j.expthermflusc.2024.111355.
- [4] Li, W., Li, H., Liu, M., Ji, L., Agarwal, R.K., Jin, S. Energy dissipation mechanism of tip-leakage cavitation in mixed-flow pump blades. *Phy Fluids* 36 015115 (2024) DOI:10.1063/5.0183540.
- [5] Ji, L., Pu, W., Li, W., Shi, W., Tian, F., Yang, Y. et al. Flow instability in mixed-flow/axial-flow pump: A review of relationship between tip leakage flow distortion and rotating stall. *P I Mech Eng A-Pow* 239, 225-253 (2024) DOI:10.1177/09576509241287838.
- [6] Al-Obaidi, A.R., Alhamid, J. Experimental and simulation analyses of the hydraulic complex internal flow characteristics in an axial pump based on varying frequency vibration ranges technique. *Int J Interact Des Manuf* 19 3661-3681 (2025) DOI:10.1007/s12008-024-02012-9.
- [7] Al-Obaidi, A.R., Alhamid, J. Investigation of the main flow characteristics mechanism and flow dynamics within an axial flow pump based on different transient load conditions. *Iran Sci Technol Trans Mech Eng* 47 1397-1415 (2023) DOI:10.1007/s40997-022-00586-x.
- [8] Al-Obaidi, A.R., Alhamid, J. Analysis of unsteady internal flow characteristics in axial pump with varying number of blades using computational modelling and vibration techniques. *Flow Meas Instrum* 99 102654 (2024) DOI:10.1016/j.flowmeasinst.2024.102654.
- [9] Al-Obaidi, A.R. Effect of different guide vane configurations on flow field investigation and performances of an axial pump based on CFD analysis and vibration investigation. *Exp Tech* 48 69-88 (2024) DOI:10.1007/s40799-023-00641-5.
- [10] Al-Obaidi, A.R. Experimental diagnostic of cavitation flow in the centrifugal pump under various impeller speeds based on acoustic analysis method. *Arch Acoust* 48 159-170 (2023) DOI:10.24425/aoa.2023.145234.
- [11] Giljen, Z., Nedeljković, M., Cheng, Y. The Influence of pump-turbine specific speed on hydraulic transient processes. *Stroj vestn-J Mech E* 70 231-246 (2024) DOI:10.5545/sv-jme.2023.776.
- [12] Kilavuz, F., Kiral, B.G. Design optimization of mechanical valves in dishwashers based on the minimization of pressure losses. *Stroj vestn-J Mech E* 70 194-208 (2024) DOI:10.5545/sv-jme.2023.768.
- [13] Li, W., Yan, G. Q., Yang, Y., Yi, Y., Ji, L., Shi, W. et al. Optimization of pump transient energy characteristics based on response surface optimization model and computational fluid dynamics. *Appl Ener* 362 123038 (2024) DOI:10.1016/j.apenergy.2024.123038.
- [14] Namazizadeh, M., Gevari, M., Mojaddam, M., Vajdi, M. optimization of the splitter blade configuration and geometry of a centrifugal pump impeller using design of experiment. *J Appl Fluid Mech* 1, 89-101 (2020) DOI:10.29252/jafm.13.01.29856.
- [15] Zhu, D., Xiao, R., Yao, Z., Yang, W., Liu, W. Optimization design for reducing the axial force of a vaned mixed-flow pump. *Eng Appl Comp Fluid* 14 882-896 (2020) DOI:10.1080/19942060.2020.1749933.
- [16] Liu, Z., Xu, L., Jia, X., Wu, J., Wang, D. Analysis of liquid flow and axial force calculation in axial clearance for floating impeller of centrifugal pump. *Trans Chinese Soc Agri Eng* 29 79-85 (2013) DOI:10.3969/j.issn.1002-6819.2013.12.011.
- [17] Dong, W., Liu, Z., Dong, Y., Yang, Z., Lu, Q., Li, Q. Study on pressure distribution of pump chamber and axial force in particle-laden flow of centrifugal pump. *P I Mech Eng A Pow* 236 831-839 (2022) DOI:10.1177/09576509211047655.
- [18] Cao, W., Dai, X., Hu, Q. Effect of impeller reflux balance holes on pressure and axial force of centrifugal pump. *J Cent South Univ* 22 1695-1706 (2015) DOI:10.1007/s11771-015-2688-2.
- [19] Cui, B., Li, J., Zhang, C., Zhang, Y. Analysis of radial force and vibration energy in a centrifugal pump. *Math Probl Eng* 2020 6080942 (2020) DOI:10.1155/2020/6080942.
- [20] González, J., Parrondo, J., Santolaria, C., Blanco, E. Steady and unsteady radial forces for a centrifugal pump with impeller to tongue gap variation. *J Fluid Eng-T ASME* 128 454-462 (2006) DOI:10.1115/1.2173294.
- [21] Ou, M., Shi, W., Jia, W., Fu, Q. Numerical simulation and experimental validation on hydrodynamic radial force of mixed-flow pump impeller. *T Chin Soc Agric Eng* 31 71-76 (2015) DOI:10.11975/j.issn.1002-6819.2015.09.012.
- [22] Zhu, L., Jin, Y., Li, Y., Jin, Y., Wang, Y., Zhang, L. Numerical and experimental study on aerodynamic performance of small axial flow fan with splitter blades. *J Therm Sci* 22 333-339 (2013) DOI:10.1007/s11630-013-0632-z.
- [23] Liang, Z., Wang, J., Jiang, B., Zhou, B., Yang, W., Ling, J. Large-eddy simulation of flow separation control in low-speed diffuser cascade with splitter blades. *Processes* 11 3249 (2023) DOI:10.3390/pr1113249.
- [24] Clark, C., Pullan, G., Curtis, E., Goenaga, F. Secondary flow control in low aspect ratio vanes using splitters. *J Turbomach* 139 091003 (2017) DOI:10.1115/1.4036190.
- [25] Yan, P., Chu, N., Wu, D., Cao, L., Yang, S., Wu, P. Computational fluid dynamics-based pump redesign to improve efficiency and decrease unsteady radial forces. *J Fluid Eng* 139 011101 (2017) DOI:10.1115/1.4034365.
- [26] Zeng, G., Li, Q., Wu, P., Qian, B., Huanh, B., Li, S. et al. Investigation of the impact of splitter blades on a low specific speed pump for fluid-induced vibration. *J Mech Sci Tech* 34 2883-2893 (2020) DOI:10.1007/s12206-020-0620-7.
- [27] Xie, S., Dai, K. Investigation on the added mass effect of centrifugal impellers with splitter blades. *3rd International Conference on Mechanical Design and Simulation* 12639 278-285 (2023) DOI:10.1117/12.2682032.
- [28] Ji, L., Li, W., Shi, W., Agarwal, R.K. Application of Wray-Agarwal turbulence model in flow simulation of a centrifugal pump with semi-spiral suction chamber. *J Fluid Eng* 143 031203 (2021) DOI:10.1115/1.4049050.
- [29] Li, W., Ji, L., Li, E., Shi, W., Agarwal, R., Zhou, L. Numerical investigation of energy loss mechanism of mixed-flow pump under stall condition. *Renew Energy* 167 740-760 (2021) DOI:10.1016/j.renene.2020.11.146.
- [30] Ji, L., Li, W., Shi, W., Tian, F., Agarwal, R. Diagnosis of internal energy characteristics of mixed-flow pump within stall region based on entropy production analysis model. *Int Commun Heat Mass* 117 104784 (2020) DOI:10.1016/j.icheatmasstransfer.2020.104784.
- [31] Ji, L., Li, W., Shi, W., Chang, H., Yang, Z. Energy characteristics of mixed-flow pump under different tip clearances based on entropy production analysis. *Energy* 199 117447 (2020) DOI:10.1016/j.energy.2020.117447.
- [32] Yu, H., Wang, T., Dong, Y., Gou, Q., Lei, L., Liu, Y. Numerical investigation of splitter blades on the performance of a forward-curved impeller used in a pump as turbine. *Ocean Eng* 281 114721 (2023) DOI:10.1016/j.oceaneng.2023.114721.
- [33] Song, H., Zhang, J., Huang, P., Cai, P., Cai, H., Cao, P. Analysis of rotor-stator interaction of a pump-turbine with splitter blades in a pump mode. *Mathematics* 8 1465 (2020) DOI:10.3390/math8091465.

- [34] Siddique, M., Samad, A., Hossain, S. Centrifugal pump performance enhancement: Effect of splitter blade and optimization. *P I Mech E A-J Pow* 236 391-402 (2022) DOI:10.1177/095765092111037407.
- [35] Khalafallah, M.G., Saleh, H.S., Ali, S.M., Abdelkhalek, H.M. CFD investigation of flow through a centrifugal compressor diffuser with splitter blades. *J Eng Appl Sci* 68 43 (2021) DOI:10.1186/s44147-021-00040-w.
- [36] Ji, L., Li, W., Shi, W., Tian, F., Agarwal, R. Effect of blade thickness on rotating stall of mixed-flow pump using entropy generation analysis. *Energy* 236 121381 (2021) DOI:10.1016/j.energy.2021.121381.
- [37] Ji, L., He, S., Li, Y., Li, W., Shi, W., Li, S. et al. Investigation of energy loss mechanism of shroud region in A mixed-flow pump under stall conditions. *P I Mech E-A Pow* 237 1235-1250 (2023) DOI:10.1177/09576509231162165.
- [38] Li, W., Huang, Y., Ji, L., Ma, L., Agarwal, R.K., Awais, M. Prediction model for energy conversion characteristics during transient processes in a mixed-flow pump. *Energy* 271 127082 (2023) DOI:10.1016/j.energy.2023.127082.
- [39] Li, W., Li, S., Ji, L., Li, E., Shi, W., Agarwal, R. et al. Effect of inlet elbow on rotation stall in waterjet propulsion pump. *Fund Res* 4 898-906 (2024) DOI:10.1016/j.fmre.2022.05.029.
- [40] Li, W., Liu, M., Ji, L., Wang, Y., Awais, M., Hu, J. et al. Research on the matching characteristics of the impellers and guide vanes of seawater desalination pumps with high capacity and pressure. *J Marine Sci Eng* 10 115 (2022) DOI:10.3390/jmse10010115.
- [41] Ji, L., Li, W., Shi, W., Tian, F., Li, S., Agarwal, R. Influence of different blade numbers on the performance of "saddle zone" in a mixed flow pump. *P I Mech Eng A-J Pow* 236 477-489 (2022) DOI:10.1177/09576509211046074.
- [42] Zhu, Z., Lin, Y., Li, X., Zhai, L., Lin, T. Axial thrust instability analysis and estimation theory of high speed centrifugal pump. *Phys Fluids* 34 075118 (2022) DOI:10.1063/5.0098194.

Acknowledgments The work was sponsored by the Science and Technology Plan Project of Chuzhou (2024CX007) and Research Initiation Fund Project of Chuzhou University (2023qd21).

Received: 2024-12-28, **revised:** 2025-03-27, **2025-04-02,**
accepted: 2025-04-09 as *Original Scientific Paper*.

Conflict of interest The authors declared that they have no conflicts of interest to this work.

Data Availability The data supporting the findings of this study are included in the article.

Author Contribution Qijiang Ma: Writing- original draft, Writing - review & editing, Software, Conceptualization. Zhenbo Liu: Writing- original draft, Writing - review & editing, Supervision. Sen Jiang: Writing- original draft, Writing - review & editing.

Raziskava vpliva dolžine vmesnih lopatic na radialne in aksialne sile v centrifugalni črpalki

Povzetek Za izboljšanje obratovalne stabilnosti centrifugalnih črpalk ta študija preučuje vpliv dolžine vmesnih lopatic na aksialne in radialne sile v centrifugalnih črpalkah. S pomočjo SST k- ω turbulentnega modela in eksperimentalne analize smo primerjali karakteristiko, aksialno silo, radialno silo ter časovno-frekvenčne značilnosti pulziranja tlaka med rotorji brez vmesnih lopatic in rotorji z vmesnimi lopaticami dveh različnih dolžin. Rezultati kažejo, da prvotni rotorji dosegajo višjo učinkovitost v bližini točke največjega izkoristka. Vendar pa pod pogoji nizkega pretoka usmerjanje toka z vmesnimi lopaticami omogoča, da rotorji z vmesnimi lopaticami dosegajo višji izkoristek. Pri rotorjih z vmesnimi lopaticami aksialna sila kaže periodičnost z dvema vrhovoma – enim večjim in enim manjšim – znotraj vsakega cikla. Dodatek vmesnih lopatic povzroči spremembo radialne sile na rotor, kar zahteva povečanje nosilnosti in togosti rotorskega sistema. Poleg tega vmesne lopaticice vplivajo na tlačne pulzacije na vstopu in izstopu iz rotorja; prvotni rotor izkazuje tlačne pulzacije pri frekvenci 145 Hz, kar pa je pri rotorjih z vmesnimi lopaticami drugače. Tako lahko rotorji z vmesnimi lopaticami zmanjšajo frekvenčne pulzacije in izboljšajo pretočne pogoje. Študija daje pomemben teoretični vpogled in podatkovno podporo za hidravlično konstrukcijsko optimizacijo centrifugalnih črpalk.

Ključne besede centrifugalna črpalka, aksialna sila, radialna sila, dolžina vmesnih lopatic, tlačne pulzacije